POLYPUBLIE

Optimizing fast-scan cyclic voltammetry for the analysis of 17-β estradiol and its interactions with dopamine

Edith Mariez, Raphaël Trouillon

Document en libre accès dans PolyPublie
Open Access document in PolyPublie

Date	2025
Type	Article de revue / Article
Version	Version officielle de l'éditeur / Published version
URL de PolyPublie **PolyPublie URL**	https://publications.polymtl.ca/64716/
Évaluation par les pairs **Peer reviewed**	Révisé par les pairs / Refereed
Conditions d'utilisation **Terms of use**	Creative Commons Attribution 4.0 International (CC BY)
Référence **Citation**	Mariez, E., & Trouillon, R. (2025). Optimizing fast-scan cyclic voltammetry for the analysis of 17-β estradiol and its interactions with dopamine. Neuroelectronics, 2(1), 0004 (26 pages). https://doi.org/10.55092/neuroelectronics20250004

Publication officielle
Official publication

Titre de la revue **Journal title**	Neuroelectronics (vol. 2, no. 1)
Maison d'édition **Publisher**	ELSP
URL officielle **Official URL**	https://doi.org/10.55092/neuroelectronics20250004
Mention légale **Legal notice**	©2025 by the authors. Published by ELSP. This work is licensed under a Creative Commons Attribution 4.0 International License, which permits unrestricted use, distribution, and reproduction in any medium provided the original work is properly cited.

Ce fichier a été téléchargé à partir de PolyPublie, le dépôt institutionnel de Polytechnique Montréal
This file has been downloaded from PolyPublie, the institutional repository of Polytechnique Montréal
https://publications.polymtl.ca

Article | Received 29 January 2025; Accepted 9 April 2025; Published 15 May 2025
https://doi.org/10.55092/neuroelectronics20250004

Optimizing fast-scan cyclic voltammetry for the analysis of 17-βEstradiol and its interactions with dopamine

Edith Mariez[1] and Raphaël Trouillon[1,2,3,*]

[1] Electrical Engineering Department, Polytechnique Montréal, Montréal, Canada
[2] TransMedTech Institute, Montréal, Canada
[3] SNC Research Group, Montréal, Canada

* Correspondence author; E-mail: raphael.trouillon@polymtl.ca.

Highlights:

- Quantitative, real-time detection of neurotransmitters.
- Impact of 17-βEstradiol on the dopamine signal.
- Optimisation of neuroanalysis.

Abstract: 17-βEstradiol (E2) and dopamine (DA) are biologically significant molecules, with E2 playing critical roles in female sexual development and neuroprotection, and DA being essential for cognitive processes and motor functions. The co-detection of these molecules is of particular interest due to their potential interactions and combined effects on neurological health. Understanding the interactions between E2 and DA is therefore essential to elucidate E2 neuromodulation, but current detection techniques are limited. Fast-scan cyclic voltammetry (FSCV) is a simple and effective electrochemical method that allows for real-time codetection of neurotransmitters and hormones. In this study, FSCV parameters are optimized for the simultaneous electrochemical co-detection of E2 and DA, using carbon fiber microelectrodes (CFMEs) for their high spatial resolution and biocompatibility. The results reveal that E2 exhibits unique electrochemical behavior which can be distinguished from DA through optimized FSCV settings, allowing for their simultaneous detection. Redox interactions altering the DA measurements are also suggested, possibly owing to the antioxidant properties of E2. This study not only enhances the understanding of the electrochemical properties of E2 and DA but also demonstrates the potential of FSCV in investigating their interactions and roles in neuroprotection and oxidative stress. Understanding the chemical interactions between these two species is also critical to guarantee accurate FSCV measurements, especially as FSCV is being increasingly considered to provide neurochemical feedback in AI-based, closed-loop neuroelectronics.

Keywords: neurotransmitter; electroanalysis; fast scan cyclic voltammetry; carbon fiber; 17-βEstradiol; dopamine



Copyright©2025 by the authors. Published by ELSP. This work is licensed under a Creative Commons Attribution 4.0 International License, which permits unrestricted use, distribution, and reproduction in any medium provided the original work is properly cited.

1. Introduction

17β-Estradiol (E2) is a steroid hormone belonging to the estrogen family. Being the most important hormone in females, it has multiple biological roles, particularly in sexual development [1, 2]. An abnormal concentration of E2 is usually associated with several health issues in children's growth, in the development of sexual characteristics, and in reproduction [2]. High levels of E2 are risk factors for breast and ovarian cancers [3], lung cancer [4], uterus and prostate cancers [5], whereas E2 deficiency promotes the development of heart diseases and is associated with the presence of menopausal symptoms and osteoporosis [6, 7].

Estrogens are also involved in a wide range of brain functions, such as cognition, memory, neurodevelopment, and neuroplasticity [8, 9]. Several studies have demonstrated that dysregulation of E2, with abnormally low concentrations, is involved in the development of psychological disorders such as schizophrenia, bipolar disorder, depression, autism, attention deficit hyperactivity disorder, anxiety, eating disorders, and substance abuse [7–10]. E2 has been found to have neuroprotective effects, possibly through its anti-inflammatory properties. The neuroprotective effects of E2 are mainly due to its intrinsic antioxidant properties, whereby estrogens act independently of their own hormonal role [11–15]. Among steroid molecules, only estrogens can prevent neuronal cell death caused by significant oxidative stress [12, 15, 16]. E2 itself acts as an antioxidant by scavenging free radicals primarily due to the free phenolic hydroxyl function on the A-ring [12], and can be regenerated after scavenging free radicals [17]. Additionally, estrogens demonstrate metal redox chelation mechanisms: they can bind to a metal ion, forming a stable complex [18].

Dopamine (DA) is one of the most important neurotransmitters in humans as it is involved in numerous cognitive processes such as memory, learning, motor function, mood, sleep and concentration [19–23]. Pathological concentrations of DA are involved in the development of many neurological diseases such as schizophrenia, Parkinson's and Alzheimer's disease, senile dementia, depression, stress, and hyperactivity, confirming the crucial role of this neurotransmitter in mental health [24]. DA is also strongly implicated in addiction processes and is a key target for the activity of cocaine or amphetamine [25].

E2 also acts as a neuromodulator on the serotonergic, glutamatergic, and dopaminergic systems [10]. Several studies have linked E2 and DA. Indeed, an increase in E2 promotes the presynaptic release of dopamine (DA) in the dorsal striatum [26], thereby enhancing memory performance with the upregulation of the catechol-O-methyltransferase gene, a gene that modulates basal prefrontal DA [27]. E2 also increases DA synthesis and decreases its turnover in the nucleus accumbens, possibly regulates the densities and functions of D1 and D2 DA receptors, and extends the duration of neurotransmission by reducing the density of membranous DA transporters responsible for DA reuptake post-exocytosis in the nucleus accumbens [9]. E2 modulates the mesolimbic DA system in female rats, and a high concentration of E2 is associated with increased motivation for sexual activity and decreased motivation for food [28]. The numerous neurological correlations between DA and E2, and the neuromodulatory effect of E2 on the dopaminergic system suggest a strong interaction between these two molecules.

However, and even though the neuromodulatory effects of E2 are now well-supported, the

interactions between E2 and DA remain poorly understood, due to a scarcity of analytical methods to codetect them with sufficient time resolution (100 ms to few s [29]). Therefore, there is a need for E2 codetection with neurotransmitters such as DA to better understand their interplay and thus their effects on mental health. In this context, electroanalytical techniques offer numerous advantages, such as rapid response times, miniaturization capabilities, and simple use and maintenance [30]. Table S1 in the Supplementary Information (SI) lists some techniques available for DA and E2 detection. These techniques are based on a redox reaction, *i.e.* an exchange of electrons, between the molecule of interest and an electrode inserted in the sample [31]. Compared to commonly used detection methods like mass spectroscopy (MS) or immunoassays (enzyme-linked immunosorbent assay, chemiluminescence immunoassay, radioimmunoassay), electrochemical methods provide comparable reliability, precision, and detection limits without requiring complex and expensive equipment [32]. Additionally, they require little or no sample preparation which minimizes the risk of errors and reduces the duration of the analysis. Electrochemical techniques are often eco-friendly, as they use simpler equipment and materials to produce and pose fewer health risks [33]. Biosensors are a promising novel method to detect E2, but many of these devices remain proof-of-concept and are used only for the detection of E2 in water samples, as they are rarely employed for the co-detection of multiple species, despite their improved sensitivity and detection limits [34].

Compared to other analytical techniques, fast scan cyclic voltammetry (FSCV) allows real-time measurement and identification of neurotransmitters and hormones in complex samples or *in vivo* [35]. During FSCV, the potential of the electrode is rapidly ramped (scan rate SR 100 to 1000 $V \cdot s^{-1}$) and cycled typically 10 times per second. Each of these cycles (cyclic voltammograms or CV) provides a description of the electrochemical properties of the sample as redox molecules are oxidised or reduced. Compared to amperometry [36], FSCV has a lower temporal resolution (100 ms *vs.* 1 ms, respectively), but it offers the possibility to simulatenously screen for different analytes, thus providing a unique mapping of the chemical dynamics of the sample [37]. FSCV has a higher chemical selectivity than CV, square wave voltammetry (SWV), or differential pulse voltammetry (DPV), with very rapid response times that make it the most suitable technique for *in vivo* monitoring of neurotransmitters with fast dynamics [37]. SWV and DPV scans also typically last one minute, which prevents them from detecting the fast, sometimes sub-second events of the brain chemistry. Carbon fiber microelectrodes (CFMEs) that have dimensions on the order of few μm are typically used with this technique, thus allowing for very fine spatial resolution. Among its many advantages, carbon is also highly biocompatible, cost-effective, inert, and particularly stable both chemically and electrochemically [38]. It exhibits good electrical conductivity, has a low background current, and can be utilized over a wider potential range compared to metals [38]. Additionally, carbon surfaces facilitate the adsorption of several neurotransnmitters, such as DA, due to the presence of functional groups [38]. FSCV has been extensively applied to and optimized for DA detection, which has allowed understanding of numerous biological action mechanisms [39–43]. Additionally, DA has been codetected with several molecules, such as serotonin (5-HT) and 3,4-dihydroxyphenylacetic acid (DOPAC) [44] or ascorbic acid (AA) [35], which has enabled the understanding of chemical interactions between DA and these molecules, and the resulting variations in measured CV. The real-time description of the chemistry of the brain offered by FSCV is expected to be crucial in the development of

neuroelectronic therapeutic solutions. For instance, it has been proposed that FSCV can help improve the input parameters in deep brain stimulations (DBS) [45–48]. FSCV measurements in humans during DBS showed the neurochemical alterations triggered by the technique [49]. Recently, FSCV was combined to a neurostimulator and artificial intelligence (AI) in a closed-loop DBS system [50]. FSCV is therefore a strong candidate to improve AI-based neuroelectronics. Potential chemical interactions should be fully understood to guarantee the efficacy of the device.

Recently Weese et *al.* detected E2 with FSCV [51], and successfully codetected E2 with DA using a modified 'shark fin' waveform in FSCV [52]. As oxidation potentials of DA and E2 are close, and because DA oxidation current is higher, the DA peak rapidly obscures the E2 one. By setting the SR at 200 $V \cdot s^{-1}$ up to 0.7 V, and by increasing it to 1000 $V \cdot s^{-1}$, both peaks were successfully separated and E2 electrochemistry was enhanced. This approach was validated in tissue matrix. However, despite this successful demonstration, the E2 electrochemical response is still not well-understood in both FSCV and CV, especially on CFMEs. The possibility to detect E2 on bare carbon fibers, *i.e.* without chemical modifications granting specificity towards E2, is important as it allows for the codetection of different analytes and thus to better understand the complex chemical interplays in the brain.

Here, the impact of the potential range used during voltammetric detection of E2, in the presence or absence of DA, is studied. The novelty of this approach is to compare results obtained at both slow (CV) and fast (FSCV) scan rates to identify the waveform parameters altering E2 detection and propose new strategies for improving E2 FSCV. By investigating the influence of negative or positive potential electrode control and/or conditioning on E2 electroanalysis, especially through adsorption behaviours, new FSCV waveforms can be designed to improve E2 detection. Indeed, other modified waveforms suggested in the literature [52] are highly specific and optimized for DA and E2 codetection. However, this specificity may limit their applicability to the codetection of E2, DA and other compounds such as 5-HT or other catecholamines. Identifying a potential waveform that would control the E2 redox behaviour in FSCV without dramatically altering the shape of the input potential waveform would be beneficial for multianalyte investigations of E2. Furthermore, the possibility of electrochemical interferences between E2 and DA altering the signal was also investigated. Indeed, the increasing body of evidence supporting the neuroprotective effect of E2 hints at a purely chemical role of E2 in the brain, beyond its hormonal activity. The possibility of redox interactions and secondary reactions, especially in the context of the antioxidant properties of E2, were to the best of our knowledge not investigated. The chemical properties of E2—or antioxidant properties, namely free radical scavenging, regeneration, and metal chelation [53]—that contribute to its neuroprotective effect are particularly interesting in the context of electrochemical codetection with DA. Indeed, a potential toxicity pathway of DA is *via* oxidative stress, as free oxidised DA can react with nearby thiol-containing molecules or the nucleophilic protein side chains, thus potentially inactivating cellular machinery [54, 55]. Several neural proteins have been identified as targets for this reaction and could be involved in neurodegeneration [55]. DA can undergo auto-oxidation to form quinonic species, which could potentially interact with E2 or its oxidation products, leading to changes in CV when the two molecules are codetected in FSCV. A redox interaction between DA and E2, either through complex formation or redox mediation, as is the case between DA and ascorbic acid (AA) [35], could shine a new light on the role of E2 in the brain.

2. Methods

2.1. Chemical reagents

All the reactants were purchased from Millipore-Sigma (Canada), unless specified otherwise. Deionized water (resistivity > $18 M\Omega \cdot$ cm) was used for preparing solutions throughout the study. 1 mM stock solutions of E2 were prepared in ethanol, stored at 4 °C and used within 30 days. Daily working solutions were made from stock by dilution in phosphate-buffered saline solution (PBS 1X, pH = 7.4), containing 2 mM NaH_2PO_4, 10 mM Na_2HPO_4, 140 mM NaCl, and 3 mM KCl. All CV and FSCV measurements were run at room temperature, and in 10 μM of E2 unless specified otherwise. 1% ethanol in PBS was used for background measurement in FSCV. For the limit of detection (LoD) measurements, the 10 mM stock solution of E2 in ethanol was diluted in PBS daily to a working solution of 100 μM. Further dilutions (500 nM, 1, 5, 10, and 50 μM) were then prepared with 1% ethanol in PBS. The DA solutions were prepared by dilution in 1% ethanol in PBS.

2.2. Carbon fiber microelectrodes

CMFEs were fabricated as previously reported in the literature [41, 56, 57] . CFMEs were made using 7 μm-diameter T-650 carbon fibers. Carbon fibers were aspirated with a vacuum pump into glass capillary tubes (1.1 mm inner diameter, 1.5 mm outer diameter PYREX-Corning, USA). The capillaries were then pulled with a vertical Narishige PC-100 electrode puller (Tokyo, Japan). The carbon fibers were sealed in place with fluid epoxy (EPOTEK-301-2, Epoxy technology, MA, USA) and cured for 3 hours at 80°C. The carbon fibers were cut under a microscope to 100–150 μm from the glass seal. CFMEs were backfilled using 3 M NaCl before each measurement and connected with a platine wire. All the CFMEs were tested in 1 mM of hexaammineruthenium (III) chloride (RuHex) in 1 M KCl before use (data not shown). The redox potentials, redox currents, and capacitive current were analyzed with Shapiro test, Q-Q plot, and finally ANOVA test to ensure the repeatability of the fabrication process, and the validity of each CFME.

2.3. Cyclic voltammetry

All CVs were collected with a VMP-300 Potentiostat (BioLogic, France) at a scan rate of 100 m$V \cdot s^{-1}$, from the negative vertex to the positive vertex, and back, over 4 cycles. The counter electrode was a platinum wire and the reference electrode was Ag|AgCl (3M NaCl). All measurements were done in a Faraday cage to limit the electromagnetic noise.

To investigate the influence of the vertices, CVs were collected in 10 μM E2 and in PBS with 1% ethanol. First, the negative vertex was varied from -0.3 to -1.1 V (-0.1 V decrements), and the positive vertex was maintained at 1.3 V. In one set of experiments, E2 measurements were run in PBS, without ethanol, to investigate the impact of the 1% ethanol on the CVs. Then, the positive vertex was varied from 0.8 V to 1.4 V (0.1 V increments), and the negative vertex was maintained at -0.8 V.

To compare the cathodic and anodic treatments, CFMEs were pre-treated in PBS or in 10 μM E2 by applying potentials of -1.1 V (cathodic) and 1.1 V (anodic) for 7 s. Before and after each treatment, a

CV in 10 μM E2 (-0.3 V to 0.9 V and back) was collected, and a CV (-0.5 V to 0.2 V) in 1mM RuHex in 1 M KCl was run to ensure the signal evolution was not due to variation in the electrode geometry. The cathodic treatment was performed first, followed by the anodic one.

2.4. Fast-scan cyclic voltammetry

Each CFME was inserted into a microfluidic chip to form a home-built flow injection analysis system. The microfluidic chip was made with polydimethylsiloxane (PDMS) using standard soft lithographic methods [58, 59]. The cross-section of the sensing channel was 1 $mm \times 1$ mm. Experiments were conducted by delivering the analyte into the microfluidic chamber containing the electrode tip. A flow rate of 1 mL/min was obtained with a Fusion 4000X Syringe Pump (Chemyx, USA). The reference and CFE electrodes were connected to a home-made printed circuit board (PCB), adapted from Caux *et al.* [60] with an gain resistance R = 10 kΩ. The excitation waveform application and the signal acquisition were both performed using the WaveForms software and an Analog Discovery 2 oscilloscope (Diligent). The excitation waveform was repeated at 10 Hz, and the signals were sampled at 10 kHz. The electrodes were cleaned with isopropyl alcohol (IPA) for approximately 10 min, and then equilibrated in FSCV for 10 min in PBS before use.

2.5. X-ray photoelectron spectroscopy (XPS) analysis

A VG ESCALAB 250Xi photoelectron spectrometer was used for the XPS analysis, in a vacuum chamber, with charge compensation and a Mono Al Kα 1486.88 eV source. The C1s peak was fixed at 284.7 eV for charge correction.

2.6. Electrochemical analysis

Cyclic Voltammetry: For the CV measurements, data were filtered using Python with a Savitzky-Golay filter ($polyorder = 1$ and $window = 20$). The capacitance current i_c was extracted at 0 V, and a 2nd-order polynomial fit was used as a baseline for the estradiol peak analysis. Indeed, it was found that the peak often occurred at rather positive potentials, and that the current baseline itself was rising in this area. A 2nd-order polynomial was found to be a good fit and predictor for this baseline (*vs.* a linear fit), and was thus used to fit the CV and isolate the E2 peak. The oxidation potential E_{ox} and current i_{ox} were both measured. The reported i_c, E_{ox} and i_{ox} values are the mean of cycles 2 to 4. To analyze the vertex influence, i_c values were normalized with $i_{c,-0.3V}$ in when the negative vertex is changed, and with $i_{c,0.9V}$ when the positive vertex is changed. The oxidation peak shift ΔE_{ox} is calculated by subtracting $E_{ox,-0.3V}$ or $E_{ox,0.9V}$ to each E_{ox} values when the negative or postive vertex is changed, respectively. The data are reported as the mean $\pm$ the standard deviation of the samples.

Fast-Scan Cyclic Voltammetry: For the FSCV measurements, data were filtered using a forward-backward digital filter in Python ($order$ = 2, f_c = 1 kHz). The nonfaradaic current was removed *via* background subtraction by averaging 10 CVs from 2 s to 5 s before the point of injection [38]. The point of injection (*i.e.* the onset of the rise in Faradic current, when the analyte reach the electrode in the microfluidic system) was calculated with the derivative of i *vs.* t curve at maximun current. Oxidation

potential E_{ox} and current i_{ox} were extracted at 2 s, 6–8 s and 15 s after injection, and the *i vs. t* curves were normalized with the maximum i_{ox} to allow inter-electrodes comparison. The reported values of i_{ox} and E_{ox} are the mean over 3 to 10 independent measurements, ± the standard deviation of the samples.

Calibration and Limit of Detection: The literature on E2 electrochemistry, especially at carbon surfaces, shows that the reaction is highly dependent on the quality of the electrode surface. This hints at a surface-dependent reaction, probably facilitated by interactions with the electrode surface and adsorption. A model inspired from a Langmuir isotherm Eq.1 was used to fit i_{ox} [40, 61, 62] as a function of [E2]:

$$i_{ox} = \frac{\beta_1 [E2]}{\beta_2 + [E2]} \tag{1}$$

where β_1 and β_2 are the fitting parameters. For low [E2], a linear approximation can be formulated from the Langmuir isotherm theory [63]. To calculate the LoD of E2, a linear regression was computed over the i_{ox} obtained for [E2] (0, 1, 5, 10, 50 and 100 μM). The LoD is the E2 concentration associated by the calibration curve (obtained from the linear approximation) to 3 times the standard deviation of the noise to define a 99.86% confidence interval [64].

2.7. Statistics

All data were proved to follow a gaussian distribution using Shapiro tests and Q-Q plots. All data reported are presented as means ± standard deviation (SD) over *n* independent sample or electrodes. Statistical analysis was conducted with a ANOVA single factor test, then completed with a post-hoc Tukey test with a 95% confidence level.

3. Results

3.1. Impact of voltammetric vertices on E2 detection

To better understand the electrochemical behaviour of E2, the influence of the cathodic and anodic vertices, E_{neg} and E_{pos} respectively, were investigated with CV at low SR= 100 m$V \cdot s^{-1}$. Anodic potentials were not tested beyond 1.4 V to avoid water oxidation [42]. As shown in Figure 1(a), different E_{neg} were tested by fixing the positive vertex E_{pos} at 1.3 V, and designing triangular CV waveforms for E_{neg} ranging from -0.3 to -1.1 V. For testing the impact of E_{pos}, the positive vertex was changed from 0.9 to 1.4 V, while keeping E_{neg} at -0.8 V. For all the experiments, SR=100 m$V \cdot s^{-1}$. Figure 1(b) shows typical CVs obtained for different E_{neg}.

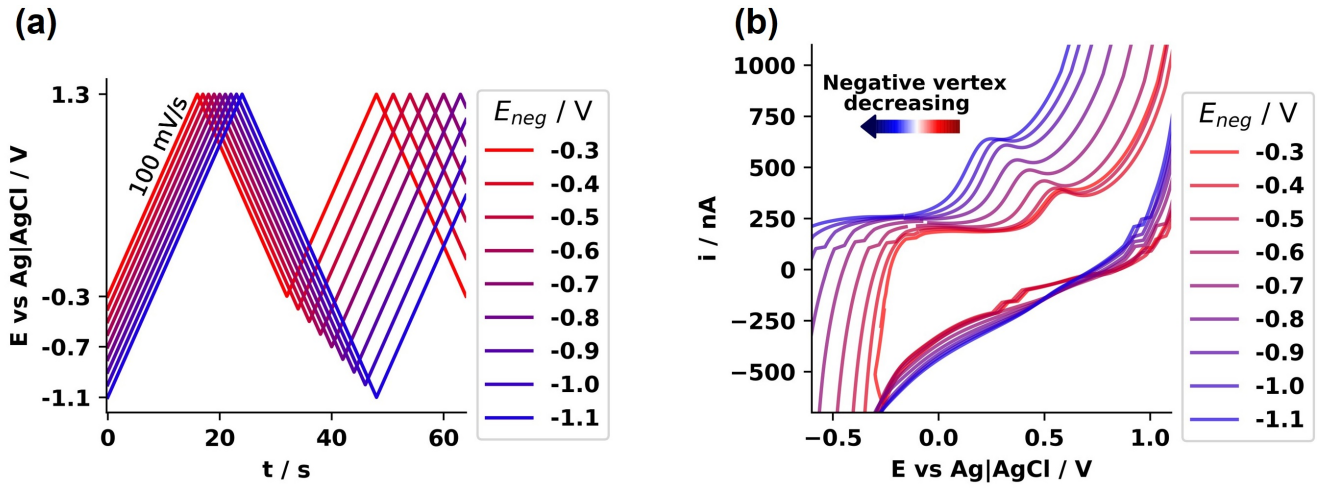


Figure 1. Negative vertex E_{neg} influence on E2 electrochemical response in CV. (**a**) Potential waveform applied for different E_{neg} (SR = 100 m$V \cdot s^{-1}$, E_{pos} = 1.3 V) and (**b**) the corresponding CVs.

During these CVs, the E2 ketone moiety is oxidized irreversibly, resulting in an inactive reaction product. The proposed reaction mechanism involves two steps, where the first electron transfer forms a phenoxy radical, before oxidizing to a phenoxium ion and then forming a ketone (see Figure 2) [65]. The reaction also involves the exchange of 2 protons. Hence, no peak appears during the reverse scan of the CV, but a wellâ€defined anodic signal is recorded [66]. E2 oxidation is adsorption- and diffusion-controlled, as there is a strong interactions between E2 and the CFME *via* π-π and electrostatic interactions and *via* hydrogen bonding [67–69].

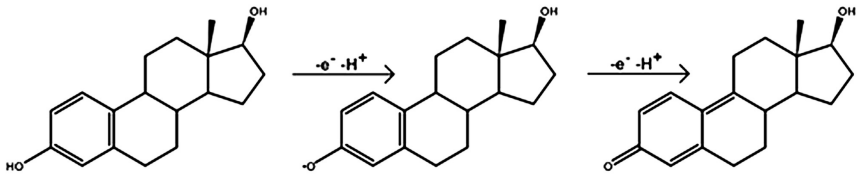


Figure 2. Proposed reaction scheme for E2 oxidation [65].

However, clear alterations to the voltammograms are observed as E_{neg} becomes more negative. The capacitive current increases while the peak potential becomes more negative. The anodic peak current also appears to rise for more negative E_{neg}, but this largely due to an increase in the baseline current.

The capacitance current i_c increased significantly for more negative E_{neg} (Figure 3(a), $p < 0.001$) and for more positive E_{pos} (Figure 3(b), $p < 0.001$). This suggests changes of the CFME or E2 adsorption effects leading to a higher density of counter ions in the double layer, either *via* an increase of the surface roughness or enhanced adsorption of E2 onto the electrode. Overall, i_c was found to be in the 1 μA range, and is $2C_{dl}SR$ where C_{dl} is the double layer capacitance [31]. From the CV data, C_{dl} was evaluated as $\sim$36 μF cm^{-2}, in good agreement with published values [70]. As a control, CVs were recorded, under similar conditions, in the background medium only, *i.e.* PBS supplemented with 1% ethanol (Figure S1 in the SI). It was found that the increase in capacitance is higher in presence of E2, possibly through local changes in pH.

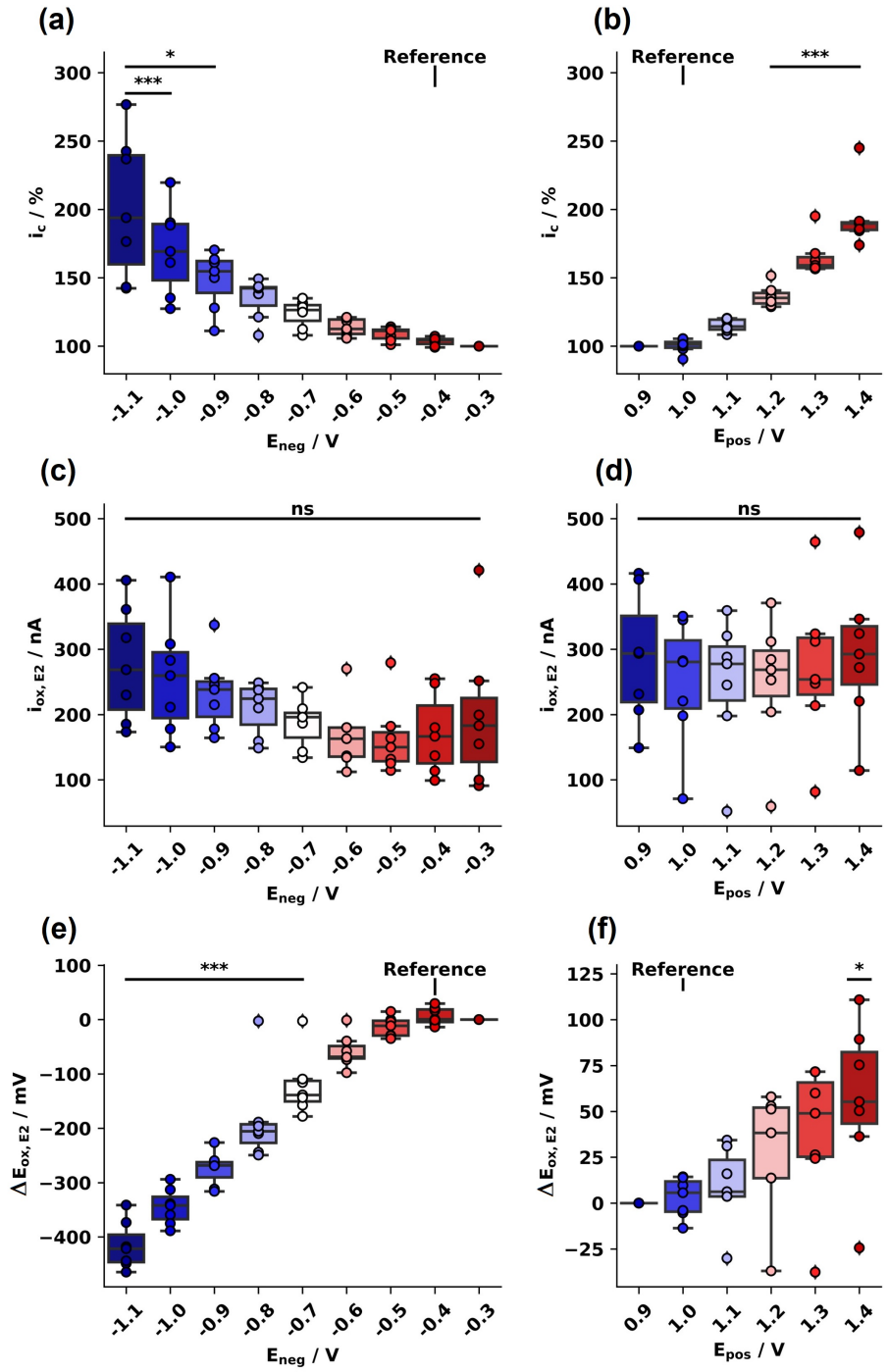


Figure 3. Variations of the capacitive current i_c with (**a**) E_{neg} and (**b**) E_{pos}. Variations of the anodic current $i_{ox,E2}$ for (**c**) E_{neg} and (**d**) E_{pos} variations. Anodic peak potential shifts $\Delta E_{ox,E2}$ for (**e**) E_{neg} and (**f**) E_{pos} variations. Post-hoc Tukey 95%, *: $p < 0.05$, **: $p < 0.01$, ***: $p < 0.001$ *vs.* the reference dataset indicated in the figures. $n = 7$.

Even though Figure 1(b) hints at an increase in $i_{ox,E2}$ with more negative E_{neg}, this parameter had no clear statistical influence on the peak current over 7 electrodes (Figure 3(c)), largely due to data variability, possibly because of E2 fouling [51]. Changes in E_{pos} had no impact on the anodic current (Figure 3(d)).

Interestingly, the anodic peak potential $E_{ox,E2}$ significantly shifted with E_{neg} (Figure 3(e), Table 1) and E_{pos} (Figure 3(f)). When E_{neg} is decreased, a linear dependence is observed from -0.5 to -1.1 V group (compared to the -0.3 V dataset, $p < 0.001$, $n = 7$), as $E_{ox,E2}$ is shifted negatively by ~400 mV as

Table 1. E2 oxidation potential for different cathodic potential (100 m$V \cdot s^{-1}$, E_{pos} = 1.4 V)

E_{neg} / V	−0.3	−0.5	−0.7	−0.9	−1.1
$E_{ox,E2}$ / mV	589 ± 35	575 ± 39	468 ± 84	315 ± 53	173 ± 32

E_{neg} becomes more negative.

Overall, this experimental dataset indicates that E2 detection with CFME is heavily dependent on the range of the potential waveform. This could be due to electrode surface alteration or E2 adsorption modulating E2 oxidation, in agreement with the literature on organic electrochemistry, for E2 or neurotransmitters [51, 71, 72]. Importantly, shifting E_{neg} negatively led to more negative $E_{ox,E2}$. This drop in the overpotential required to drive E2 oxidation hints at a facilitated reaction. Combined with the observation that the capacitive current is higher for this waveform, this could be explained by pre-adsorption of E2 on the electrode surface during the more negative part of the potential waveform, leading to enhanced oxidation kinetics. Local chemical variations in the vicinity of the electrode (pH changes, water oxidation) could also contribute to the observed effect. Conversely, E_{pos} led to $E_{ox,E2}$ shift to higher potentials, suggesting that anodic treatment makes E2 oxidation more difficult.

Accumulation time was not investigated as it appears to not influence E2 electrochemical response [73]. E2 was diluted in PBS and pH was controlled at 7.4, but it seems that lower pH enhances E2 oxidation as protons H^+ control the reaction [66, 67].

3.2. Influence of cathodic vs. anodic holding potentials

To further investigate the influence on E2 detection of surface modifications, independently from E2 adsorption effets, a cathodic and an anodic CFME pretreaments were tested. CFMEs were pretreated both in PBS and in 10 μM E2 during 7 s, applying −1.1 V and 1.1 V for cathodic and anodic pretreatments respectively, as shown in Figure 4. The pretreatments were short (7s) to avoid dramatically etching the electrode surface, which would be seen with changes in i_c. This was supported by running CV in RuHex before and after the treatments (data not shown). No variation in peak current, peak potential and capacitance were observed for the RuHex tests before and after pre-treatment which hints that the alterations observed for E2 are likely due to specific alterations in its interactions with the electrode surface rather that non specific changes in electrode surface, roughness or shape.

Anodic treatments are expected to increase the oxygen content of carbon electrodes [72], as confirmed by an XPS analysis of the CFME surface after cathodic and anodic treatments. The ratios between the magnitudes of the C1s peak to the O1s were 2.2 for the post-cathodic sample and 1.96 for the post-anodic sample, as shown in Figure 5(a), (c) and (b), (d) respectively. Thus, oxygen proportion is higher at the anodically-treated CFME surface, thus confirming the chemical alterations of the CFME surface induced by the different treatments.

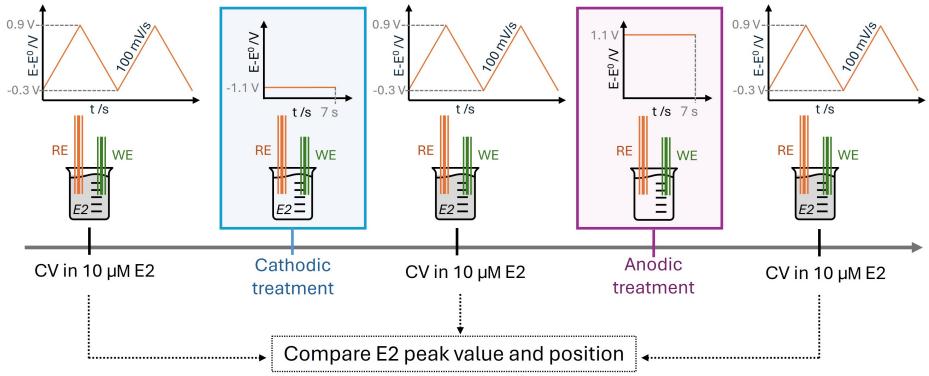


Figure 4. Schematic summarizing the sequence of cathodic and anodic pre-treaments on CFMEs in PBS and in 10 μM E2.

The E2 oxidation current $i_{ox,E2}$ was normalized with i_c to remove the surface dependency of the results, as shown in Figure 5(e). As the surface is anodically treated, it produces a more oxygenated surface, with a significant $i_{ox,E2}$ decrease of 56% $\pm$ 10% in PBS, and of 58% $\pm$ 9% in E2. Morevover, this is in agreement with previous results that E2 oxidation is hindered while increasing the positive boundary in CV (Figure 3 (f)). The presence of E2 in the pretreatment solution did not impact significantly the results. This shows that the improved behaviour of the cathodic treatment is not due to E2 accumulation during the application of the negative potential, but to intrinsinc changes in electrode surface characteristics. No significant shift was observed on $E_{ox,E2}$ suggesting that facilitated oxidation due to lower E_{neg} is mainly related to the E2 adsorption processes, that rapidly vanish when potential is not applied anymore on the CFME (Figure S2 in the SI).

Cathodic treatment thus improves the E2 electrochemical response. This confirms that decreasing the negative potential beyond -0.7 V, as seen in the previous CV experiments, is beneficial for E2 detection with CFMEs, possibly through surface changes of the electrode surface. Longer anodic treatments were tested, but all electrodes were irreversibly damaged and E2 detection was not possible after treatment. Indeed, extended anodic treatments were reported to oxidatively etch the surface of the CFME [74]. This can be a desirable effect, as the continuous etching of the surface actually cleans the electrode and maintains its sensitivity during long measurements. Here, our tests were designed to limit that etching effect, and focus only on the chemical alterations at the surface of the CFME.

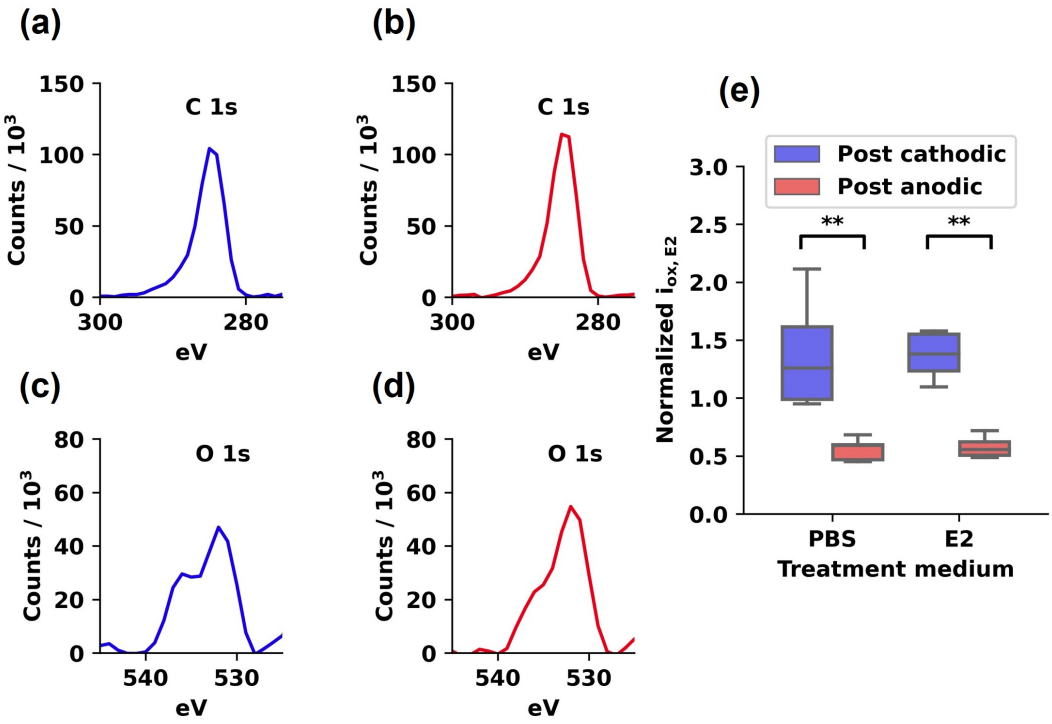


Figure 5. Cathodic and anodic treatments change the surface composition of the CFME and influences E2 oxidation. C1s peak, (**a**) post-cathodic and (**b**) post-anodic sample, and O1s peak, (**c**) post-cathodic and (**d**) post-anodic sample, obtained with XPS. (**e**) E2 oxidation current is normalized with i_c. The post-cathodic current is divided by the pre-treatment current (blue boxes), and the post-anodic current is divided by the post-cathodic current (red boxes). The E2 oxidation current increased after a cathodic treatment, and significantly decreased after an anodic treatment. No significant difference is observed in the presence or in the absence of E2 in the treatment medium. Post-hoc Tukey 95%, *: $p < 0.05$, **: $p < 0.01$, ***: $p < 0.001$, ns: not significant. $n = 5$.

3.3. Impact of the holding potential on E2 FSCV

To confirm that the results obtained above with low SR translate to FSCV, the impact of the negative boundary of the FSCV waveform on E2 detection was considered. The holding potential E_{hold} was varied from $-0.3V$ to -0.6 V while maintaining the SR at 400 $V \cdot s^{-1}$ and without any discontinuity in the potential trace, as shown in Figure 6(a). The period during which E_{hold} is applied varies from 91.25 ms to 89.75 ms while decreasing E_{hold}, which is possibly inducing a slight variation of about 3% in the duration of the holding phase. In these very short timescales, this variation was considered negligeable, especially with regards to the changes observed with the different experimental conditions (*vide infra*). A typical FSCV trace for the injection of 10 μM of E2 in PBS with 1% ethanol is presented in Figure 6(b). As the E2 enters the detection chamber, the rise of a clear anodic current (peak i. in Figure 6(b) and (c)), corresponding to the irreversible oxidation of E2, appears on the forward scan at 0.85 V.

However, and in agreement with the CV data obtained for SR = 100 m$V \cdot s^{-1}$, changes in the negative boundary of the potential waveform, here E_{hold}, had a direct influence on the position of the anodic peak. For an excitation waveform going from -0.4 V to 1.45 V, the E2 oxidation potential is 954 $\pm$ 27 mV, which is in accordance with previous results on E2 detection using FSCV [51]. As shown in Figure 6(c),

a clear negative shift of the E2 peak is recorded as E_{hold} is decreased from −0.3 V to −0.6 V. The return peak (peak ii. in Figure 6(b) and (c)), around 1.1 V on the reverse scan, has been previously described by others for the FSCV detection of E2 [51]. It has been attributed to the oxidation of the hydroxyl present on the pentyl ring of E2 to a ketone. This reverse peak was found to increase as E_{hold} decreases. As cathodic pretreatments typically enhance the detection of aromatic molecules, such as DA [41], this indicates that this reverse peak, likely arising from the oxidation of another E2 moiety, is surface-dependent and facilitated by a cathodic preconditioning of the CFME.

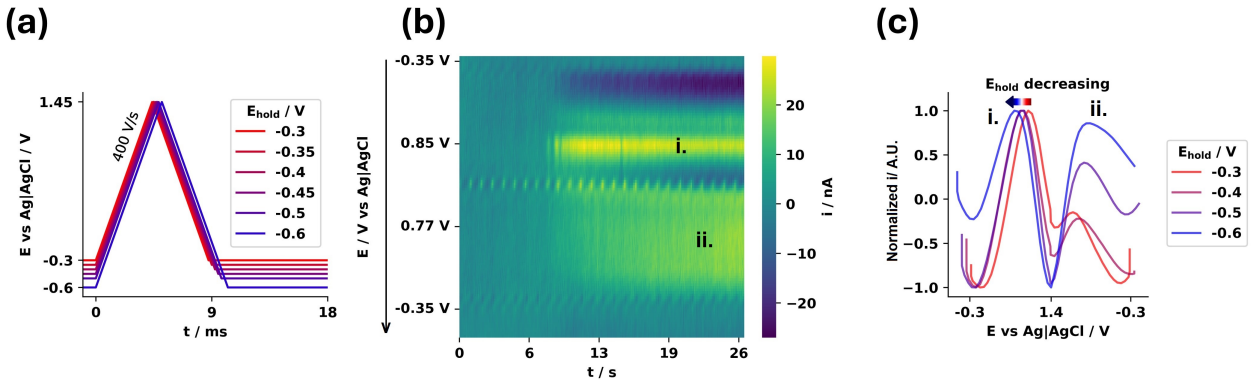


Figure 6. FSCV detection of E2 for different holding potentials E_{hold} (**a**) Input potential waveforms for different E_{hold} varied from −0.3 V to −0.6 V. During the triangular part of the wave, SR is maintained at 400 V/s^{-1} . (**b**) Typical FSCV colormap showing the detection of 10 μM of E2, as the analyte enters the detection chamber at ~7 s (E_{hold} = −0.35 V). The arrow indicates the direction of the potential scan. (**c**) Voltammograms recorded at the instant corresponding to the maximum anodic E2 current, for different E_{hold}. The recorded current was normalized to its maximum value. The labels i. and ii. identify the peaks observed in the voltammgram.

For a switching potential E_{switch} of 1.45 V, $E_{ox,E2}$ shifted significantly ($p < 0.001$) and almost linearly towards more negative values as E_{hold} decreases (Figure 7(a)). A similar trend is observed for E_{switch} = 1.35 V, but the measured $E_{ox,E2}$ are overall 80 mV higher than for E_{switch} = 1.45 V (Figure 7(b) and Table 2, $n = 3$, $p < 0.01$). Carbon surface etching has been reported for E_{switch} above 1.3 V [74, 75]. In this process, the repeated over-oxidation of the graphite surface increases its hydroxyl and carboxyl functionality content on the surface [76], enhancing its electroactivity towards, for instance, catechol-containing molecules. This is also a destructive method, as others have reported that the outer layer of the graphitic electrode is repeatedly etched [74]. As E2 fouls the electrode [51], its detection may benefit from such surface regeneration and etching.

Despite an overall increase in current as E_{hold} becomes more negative, and for E_{switch} = 1.45 V *vs.* 1.3 V, no significant variation was observed on $i_{ox,E2}$, in agreement with previous results [51] (Figure S3 in the SI).

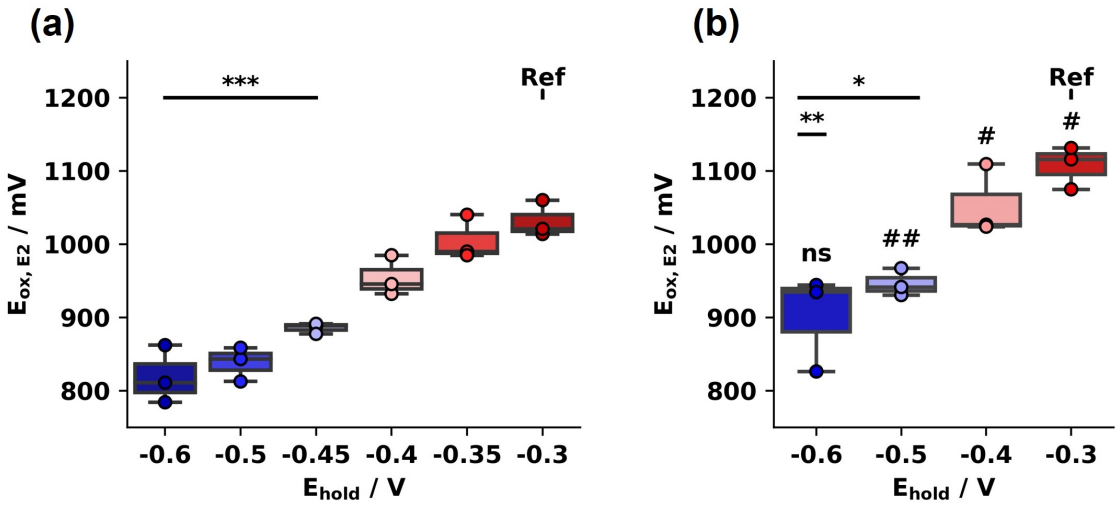


Figure 7. Impact of the holding potential E_{hold} on the position of the E2 anodic peak $E_{ox,E2}$ for a positive switching potential E_{switch} of (**a**) 1.45 V and (**b**) 1.35 V. FSCV recorded for 10 μM of E2 in PBS with 1% ethanol. Post-hoc Tukey 95%, *: $p < 0.05$, **: $p < 0.01$, ***: $p < 0.001$ *vs.* the -0.3 V dataset, and #: $p < 0.05$, ##: $p < 0.01$ when comparing datasets for the same E_{hold} but different E_{switch}. $n = 3$.

Table 2. Differences between the $E_{ox,E2}$ recorded for E_{switch} = 1.35 V and E_{switch} = 1.45 V, $\Delta E_{ox,1.35\,V\,vs.\,1.45\,V}$ for several E_{hold}.

E_{hold} / V	-0.3	-0.4	-0.5	-0.6
$\Delta E_{ox,1.35\,V vs.\,1.45\,V}$ / mV	83 ± 53	108 ± 15	99 ± 40	76 ± 24

3.4. FSCV co-detection of DA and E2

To analyse the codetection of DA and E2 and investigate the possibility of chemical redox interactions between DA and E2, the impact of E_{hold} on the FSCV traces was studied on solutions of 1 μM of DA and 5 μM of E2. As a reference, the typical waveform defined for the calibration curve (see the SI, E_{shift} = 1.45 V, E_{hold} = -0.35 V) was used. Typical voltammetric traces for 1 μM DA, 5 μM E2 and 1 μM DA with 5 μM E2 are shown in Figure 8(a) at the time corresponding to the maximum current. This corresponds to a delay of ~15 s after the moment when the analytes first reaches the electrode (see Figure 10(a)), and depends on the microchannel geometry, the dead volume, and the flow rate. At this stage, the concentrations in the chamber have reached their maximum concentration. A calibration curve for DA can be found in Figure S4 in the SI. Similarly, FSCV for different neurochemically-relevant molecules can be found in Figures S5 to S7. As previously described by Weese *et al.*, the DA peak rapidly obscures the E2 signal, making it difficult to codetect both molecules in FSCV using a standard excitation waveform, see Figure 8(a) [52].

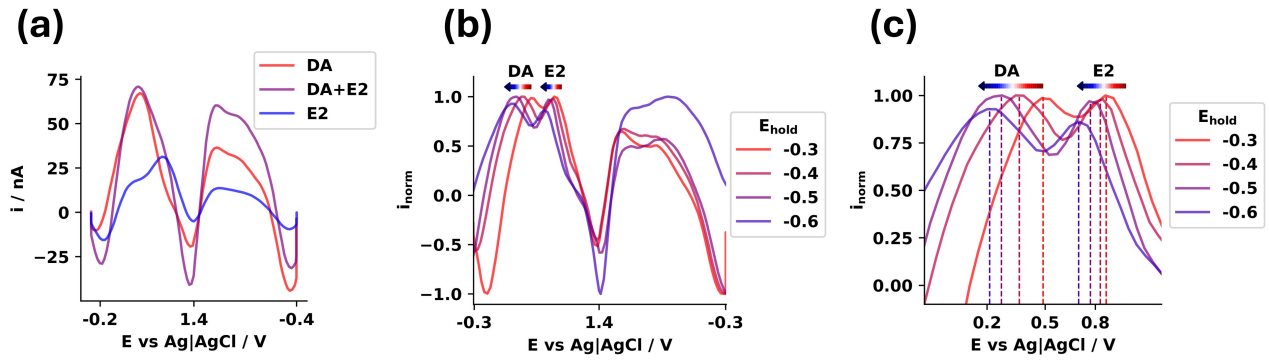


Figure 8. Codetection of E2 and DA using FSCV. (**a**) E2 peak is barely discernable when codetected with 1 μM DA (purple curve). (**b**) and (**c**) ~7 s after the injection point, E2 is more visible as the DA oxidation current increases slower than the E2 one. Both peaks shifts to lower potentials with decreasing E_{hold}.

However, if the *i vs. E* traces are now taken ~7 s after electrode first detect changes in current, E2 and DA peaks are both clearly visible, making possible to extract both oxidation potential as shown in Figure 8(b) and (c). To allow comparison over different E_{hold}, the current was normalized with the maximum recorded current in the voltammogram. DA detection kinetics is specifically discussed in the following section 3.5. Oxidation peak shift is still confirmed for E2, but also for DA as shown in Figure 8(b) and (c).

To get a better description of these potential shifts, voltammograms were extracted ~7 s after the onset of the rise in Faradic current and the position of the different peaks were measured for single and codetection. For both molecules, it is observed that the anodic peaks shift towards negative potential as E_{hold} decreases (Figure 9(a)–(c)). DA peak shifted significantly with E_{hold} variation (Figure 9(a)) as it was observed for E2 (Figure 7(a) and (b)).

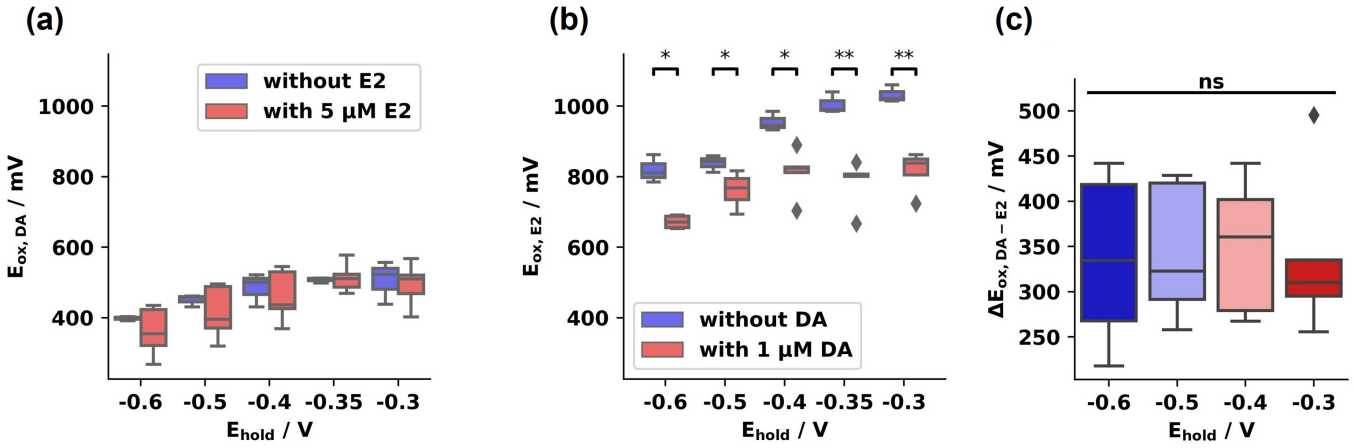


Figure 9. (**a**) In absence of E2, the $E_{ox,DA}$ shifted significantly when decreasing E_{hold} from -0.3 to -0.6 V ($n = 3$, $p < 0.001$ *vs.* the reference dataset indicated in the figure). (**b**) A significant decrease in E_{ox} is observed when detecting E2 in presence of DA ($n = 5$, $p < 0.01$). (**c**) No significant variation is observed for DA and E2 peak separation ($n = 5$). Post-hoc Tukey 95%, *: $p < 0.05$, **: $p < 0.01$, ***: $p < 0.001$, ns = not significant.

More interestingly, $E_{ox,DA}$ shift seems to be mostly unaffected by the presence of E2 (*i.e.* detected alone *vs.* codetected) as shown in Figure 9(b), with no significant difference bewteen these groups. However, E2 peak significantly shifted negatively when codetected with DA as shown in Figure 9(b) ($p < 0.01$, $n = 5$). The numerical values of $E_{ox,E2}$, for several E_{hold}, are reported in Table 3, when detecting 5 μM of E2 without or with 1 μM DA. This observation hints that E2 oxidation is altered in the presence of DA, which suggests a strong redox interaction between both molecules during FSCV codetection.

Table 3. $E_{ox,E2}$ for several E_{hold} in absence of 1 μM DA *vs.* in presence of DA.

E_{hold} / V	−0.3	−0.35	−0.4	−0.5	−0.6
$E_{ox,E2}$ / mV without DA	1032 ± 20	1005 ± 25	954 ± 22	838 ± 19	819 ± 32
$E_{ox,E2}$ / mV with DA	832 ± 59 *	784 ± 60 *	811 ± 60 *	758 ± 41 **	697 ± 53 **

Post-hoc Tukey 95%, *: $p < 0.05$, **: $p < 0.01$, ***: $p < 0.001$. when comparing when comparing $E_{ox,E2}$ datasets with *vs.* without DA for the same E_{hold}. $n = 3$.

No significant variation in the distance between the DA and E2 peaks was found when E_{hold} varies (Figure 9 (c)), thus, DA and E2 oxidation potential shifts are comparable as the experimental conditons are changed. Overall, the DA and E2 peaks separation was calculated at ~7 s after the onset of the rise in Faradic current and is 303 ± 71 mV, which is lower than Weese et *al.* [52] but sufficient to identify both peaks.

3.5. Alterations of DA detection kinetics in the presence of E2

As previously mentioned, when extracting the voltammograms at ~7 s the onset of the rise in Faradic current, E2 and DA peaks are more distinguishable. Figure 10 shows a typical FSCV colormap for the codetection of 5 μM of E2 and 1 μM of DA, with the DA oxidation peak at 0.53 V and the E2 oxidation peak at 0.81 V on the forward scan. Between ~7 s and ~15 s, it appears that the DA oxidation peak is slightly shifted to higher potentials as shown in Figure 10(b).

The $E_{ox,DA}$ shift $\Delta E_{ox,DA,\Delta t}$ between 7 and 15 s after the introduction of the analyte in the detection chamber is calculated by subtracting $E_{ox,DA,7\,s}$ at 7 s from $E_{ox,DA,15\,s}$ at 15 s after the injection point. Values of $\Delta E_{ox,DA,\Delta t}$ are reported in Table 4 for several holding potentials and for DA detection with and without the presence of E2.

Table 4. Values of $\Delta E_{ox,DA,\Delta t}$ for several E_{hold} when detecting 1 μM DA without and with 5 μM E2.

E_{hold} / V	−0.3	−0.35	−0.4	−0.5	−0.6
$\Delta E_{ox,DA,\Delta t}$ / mV without E2	9 ± 7	−4 ± 6	−8 ± 7	8 ± 5	14 ± 22
$\Delta E_{ox,DA,\Delta t}$ / mV with E2	12 ± 10	15 ± 8	6 ± 4	22 ± 4	42 ± 2

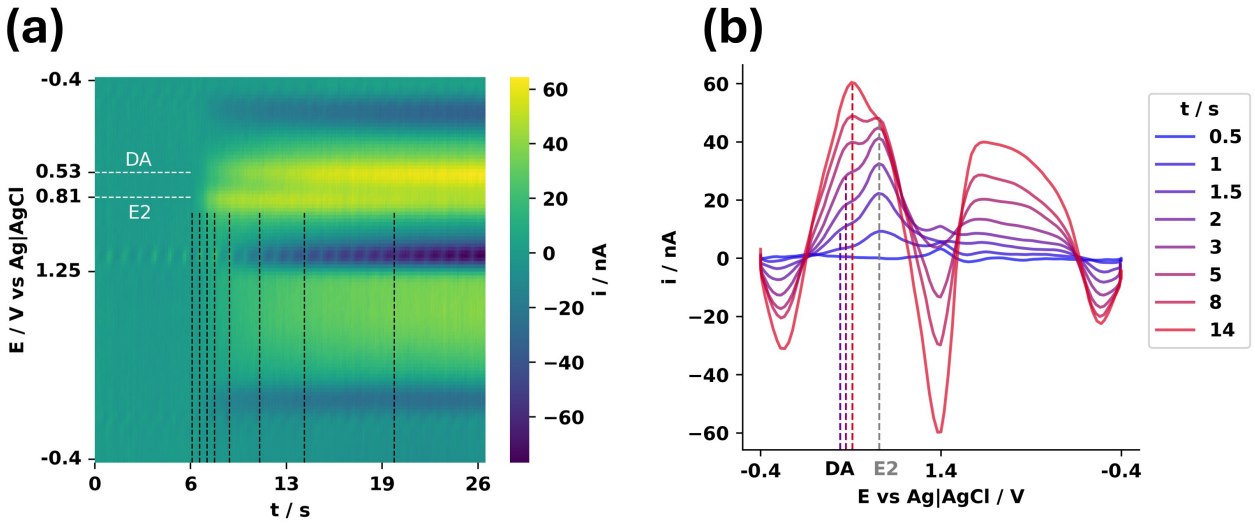


Figure 10. Codetection of E2 and DA using FSCV. (**a**) Typical FSCV colormap showing the codetection of 5 μM of E2 and 1 μM of DA, as the solution enters the detection chamber at ~6 s. (**b**) *i vs. E* is plotted at several time after analyte injection, corresponding to the black dotted lines on (**a**). The DA peak (colored vertical lines) grows more slowly than the E2 one (grey vertical line), making the latter more visible during the ~7 s after the injection. The DA peak shifts to the right over time meaning that oxidation potential is slightly more difficult.

In the absence of E2, the DA peak is not shifted during the course of the injection ($\Delta E_{ox,DA,\Delta t} = 4 \pm 15$ mV), and no significant variation is observed while decreasing the holding potential (Figure 11(a)). However, when codetecting E2 and DA , the peak of DA is pushed toward more positive values during the course of the injection of the analyte. Furthermore, a significant increase in $\Delta E_{ox,DA,\Delta t}$ was observed while decreasing E_{hold}. Indeed, from 7 s to 15 s after injection, $E_{ox,DA}$ is shifted by 12 ± 10 mV for $E_{hold} = -0.3$ V, whereas $E_{ox,DA}$ increas shifted by 42 ± 2 mV for $E_{hold} = -0.6$ V.

The DA oxidation current $i_{ox,DA}$ was extracted 15 s after the analyte injection point, for measurements in the absence or presence of 5 μM of E2 (Figure 11(b)). As a reference, each dataset at different E_{hold} was normalized with the dataset obtained with DA alone using $E_{hold} = -0.3$ V. No significant variation was observed in $i_{ox,DA}$ while decreasing E_{hold} when the DA was codetected with E2. A slight decrease in current was however observed while decreasing E_{hold} in 1 μM of DA alone.

To better consider the variations of $i_{ox,DA}$ as a function of E_{hold}, the current was fit linearly with E_{hold} as $i_{ox,DA} = \alpha\, E_{hold} + \beta$ for each electrode, in the absence or presence of E2. It was found that α is 1.1 ± 0.36 nA v^{-1} in the absence of E2 and -0.24 ± 0.67 nA v^{-1} in the presence of E2 (n = 3, $p < 0.05$ for a one-tailed Student's t-test). This further emphasizes that DA detection is altered by the presence of E2. In particular, the impact of the more negative E_{hold} is completely abolished in the presence of E2. A possible explanation could be competitive adsorption of the two molecules on the electrode surface on the same adsorption sites. As the test solution is more concentrated in E2 than DA, DA adsorption could be partially prevented by the E2 excess, thus limiting the impact of the cathodic treatment on the surface-dependent DA oxidation.

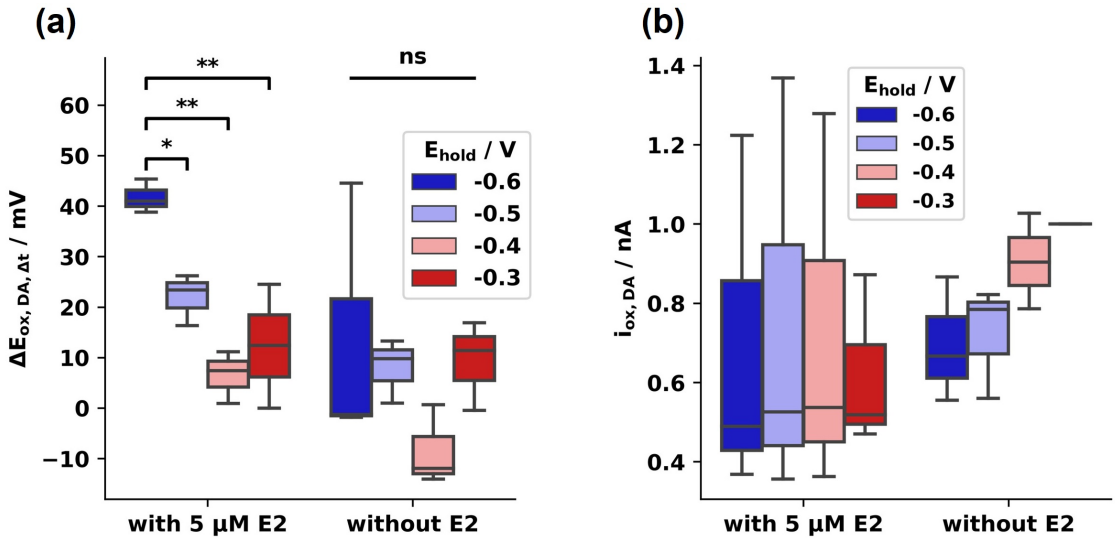


Figure 11. DA detection kinetics when detected with *vs.* without E2. (**a**) From 7 s to 15 s, a shift of $E_{ox,DA}$ to higher potentials occurs both when DA is detected with E2 and without the presence of E2. However, the shift increases significantly when E_{hold} is decreased when DA is codetected with E2. (**b**) $i_{ox,DA,7s}$. Post-hoc Tukey 95%, *: $p < 0.05$, **: $p < 0.01$, ***: $p < 0.001$. $n = 5$ in codetection $n = 3$ in DA detection alone.

To better describe the change of DA detection dynamics in the absence and presence of E2, the variations of the DA anodic currents during the injection of the analyte were considered. The $i_{ox,DA}$ *vs.* t traces were extracted from 0 s to 15 s after the injection point for n = 3–5 measurements and normalized with maximum $i_{ox,DA}$ to allow interelectrode comparison. The mean and the standard deviation of $i_{ox,DA}$ *vs.* t curves (3 to 7 measurements, $n = 3$) are presented in Figure 12 for $E_{hold} = -0.3$ V (a), $E_{hold} = -0.4$ V (b) and $E_{hold} = -0.5$ V (c).

Clear differences in DA current kinetics are observed depending on the absence or presence or E2. In the presence of E2, the DA current rises slower to its maximum. To quantify this rate of increase, the half-time $t_{1/2}$, *i.e.* the time required for the current trace to rise from 0% to 50% of its maximum, was considered for different E_{hold}, as shown in Table 5. Overall, and for all the E_{hold} considered, the $t_{1/2}$ associated to DA, $t_{1/2,DA}$, was 27% lower in the presence of E2 *vs.* for DA alone ($p < 0.05$). Furthermore, and in the presence of E2, $t_{1/2,DA}$ decreased with E_{hold} and getting closer to the $t_{1/2}$ collected for the E2 current during the codetection, $t_{1/2,E2}$.

The results shown in the previous subsections indicate that lower E_{hold} facilitates E2 detection, possibly through improved adsoprtion on the electrode surface, as hinted by the lower anodic potentials. As the delay in FSCV current rises in hydrodynamic conditions are typically associated to sluggish adsorption kinetics [40], this is supported by the lower $t_{1/2,E2}$ measured for $E_{hold} = -0.5$ V.

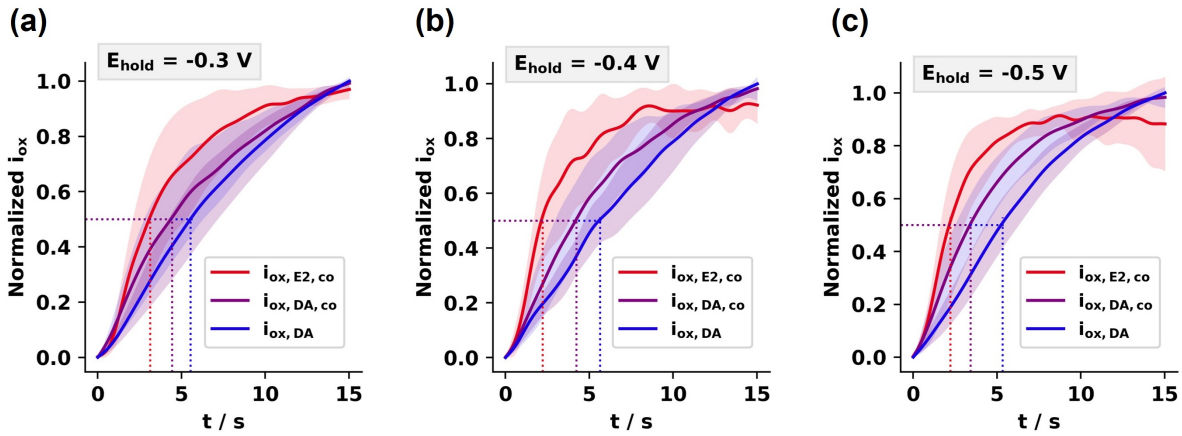


Figure 12. Dynamic response of the DA oxidative peak current for several E_{hold}. $i_{ox,DA}$ is plotted over time from the injection point to 15 s after injection. The mean ± standard deviation of $i_{ox,DA}$ *vs.* t curves (3 to 5 measurements, $n = 3$) are plotted for (**a**) $E_{hold} = -0.3$ V, (**b**) $E_{hold} = -0.4$ V, and (**c**) $E_{hold} = -0.5$ V. The currents are normalised over their maximum values.

Table 5. Rise time to the half-maximum $t_{1/2}$ for the oxidation currents of DA and E2, normalized to their maximum. Several E_{hold} were considered, for 1μM DA only, and during codetection of 1 μM DA and 5 μM E2. In this case, the $t_{1/2}$ of the currents associated to DA and E2 are reported.

	E_{hold} / V	−0.3	−0.4	−0.5	All
1μM DA only	$t_{1/2,DA}$	5.54	5.64	5.34	5.50 ± 0.13
1μM DA and 5μM E2	$t_{1/2,DA}$	4.43	4.23	3.42	4.02 ± 0.43*
	$t_{1/2,E2}$	3.12	2.21	2.21	2.52 ± 0.43***

Post-hoc Tukey 95%. *: p < 0.05, ***: p < 0.001. Comparing mean $t_{1/2}$ over several E_{hold} *vs.* the DA only dataset, $n = 3$.

Combined with the fact that the DA current rises faster in the presence of E2, especially for lower E_{hold} where E2 electrode surface adsorption is enhanced, thus possibly increasing E2 levels at the vicinity of the electrode surface, this hints that E2 directly impacts DA detection kinetics during codetection. As E_{hold} decreases, the difference between the $t_{1/2}$ for DA and E2 currents is reduced, while no variation in $t_{1/2,DA}$ is observed for DA alone. This indicates that the E2 concentration at the electrode vicinity directly increases the DA signal. Considering the antioxidant properties of E2, it is likely that the higher local levels of E2 at more negative E_{hold} reduce back the DA oxidised during the FSCV, thus regenerating it, thus locally increasing its concentration and its signal, as observed for instance with ascorbic acid [35]. The fact that the DA current kinetics during the injection follows that of E2 could be evidence for an EC' mechanism, as the DA current would then be controlled by [E2] [31]. In this case, a higher DA current would also be expected, which is not the case here. E2 is known to be a fouling species, and as DA is strongly surface dependent, it is possible that E2 and DA compete for the same fouling/ adsorption sites. Overall, these results hint that E2 modulates the DA signal via i—electrode fouling leading to lower DA currents and ii—antioxidant regeneration of the oxidised DA leading to higher currents (canceled by the fouling effect) and faster rise times. A limitation of the study is that the tests were run in a controlled, *in vitro* setup. The pH was 7.4 to match the physiological environment and its impact on E2 detection

was not considered. Several reports have detailed the mechanisms of FSCV detection *in vitro* or in fluidic setups. These studies were for instance critical to better understand adsorption processes during FSCV and optimize *in vivo* detection [40]. The application of FSCV *in vivo* has been extensively described, thus opening the possibility of studying these phenomena in an animal model [77]. CFME are typically well integrated *in vivo*, and the background subtraction approach allows for canceling the impact of the chemistry of the biological environment. However, and beyond E2, other biomolecules, such as thiols or AA, have been reported to interact with DA electrochemistry [54]. Considering the complexity of biological samples (e.g. many spectator or electroactive molecules, rapid concentration changes) will be critical to fully account for the impact of E2 on DA electrochemistry.

4. Conclusion

The detection of E2 with CFMEs was investigated at low and high SR (CV and FSCV). Importantly, the impact of the negative boundaries of the input potential waveforms on the position of the E2 oxidation peak were studied. Modulating the negative vertex (CV) of the holding potential (FSCV) all lowered the oxidation overpotential, possibly hinting at enhanced E2 electrode surface adsorption. In a similar fashion, cathodic pretreatment allowed for an enhancement of the anodic E2 current, over an anodic pretreatment, likely because structural and chemical changes at the carbon surface of the CFME mediate this improved voltammetric behaviour.

When E2 and DA were codetected, major changes in the redox behaviour of DA detection were observed. The rise in DA current was found to be faster in the presence of E2, and occured at a lower potential than in the absence of E2. Considering the neuroprotective and antioxidant properties of steroids [12, 15, 16], and especially E2, this could be evidence of redox interactions between DA and E2 during electrochemcial detection. This is relevant for neurobiology, where the role of oxidative stress and antioxidant is expected to be major factors in neurodegenerative diseases [78]. For instance, estrogens are suspected to be a major protective factor in Parkinson's disease [79]. This study hints at a possible direct chemical mechanism in the neuroprotective action of E2.

Beyond the chemical results of this study, understanding these interactions is critical to elucidate DA dynamics with FSCV, especially in the context of AI-based neuroelectronics, such as closed-loop DBS. As neuroelectronic therapeutic systems are developing rapidly, inaccurate *in vivo* DA measurements due to changes in E2 levels could lead to inadequate feedback and control in brain stimulations, and thus to poor neuroelectronic management in female patients.

Supplementary data

A file of supplementary data is provided with this article.

Acknowledgments

This research was funded by the TransMedTech Institute, the Ecole Polytechnique de Montréal, the FNFR grant number NFRFE-2022-00671, the NSERC grant number RGPIN-2023-05437 and the FRQNT grant number 312011.

Author's contribution

Conceptualization, E.M. and R.T.; methodology, E.M. and R.T.; investigation, E.M.; formal analysis, E.M.; data curation, E.M.; writing—original draft preparation, E.M. and R.T.; writing—review and editing, E.M. and R.T.; visualization, E.M. and R.T.; supervision, R.T.; project administration, R.T.; funding acquisition, R.T. All authors have read and agreed to the published version of the manuscript.

Conflicts of interests

The authors declare no conflict of interest.

References

[1] Nelson LR, Bulun SE. Estrogen production and action. *J. Am. Acad. Dermatol.* 2001, 45(3):S116–S124.

[2] Waifalkar PP, Noh D, Derashri P, Barage S, Oh E. Role of estradiol hormone in human life and electrochemical aptasensing of 17β-estradiol: a review. *Biosensors* 2022, 12(12):1117.

[3] Giulivo M, Lopez de Alda M, Capri E, Barceló D. Human exposure to endocrine disrupting compounds: Their role in reproductive systems, metabolic syndrome and breast cancer. A review. *Environ. Res.* 2016, 151:251–264.

[4] Chakraborty S, Ganti AK, Marr A, Batra SK. Lung cancer in women: role of estrogens. *Expert Rev. Respir. Med.* 2010, 4(4):509–518.

[5] Allen NE, Key TJ, Dossus L, Rinaldi S, Cust A, *et al.* Endogenous sex hormones and endometrial cancer risk in women in the European Prospective Investigation into Cancer and Nutrition (EPIC). *Endocr. Relat. Cancer* 2008, 15(2):485–497.

[6] Sherman BM, Korenman SG. Measurement of serum LH, FSH, estradiol and progesterone in disorders of the human menstrual cycle: the inadequate luteal phase. *J. Clin. Endocrinol. Metab.* 1974, 39(1):145–149.

[7] Balzer BWR, Duke SA, Hawke CI, Steinbeck KS. The effects of estradiol on mood and behavior in human female adolescents: a systematic review. *Eur. J. Pediatr.* 2015, 174(3):289–298.

[8] Russell JK, Jones CK, Newhouse PA. The role of estrogen in brain and cognitive aging. *Neurotherapeutics* 2019, 16(3):649–665.

[9] Hwang WJ, Lee TY, Kim NS, Kwon JS. The role of estrogen receptors and their signaling across psychiatric disorders. *Int. J. Mol. Sci.* 2020, 22(1):373.

[10] Bendis PC, Zimmerman S, Onisiforou A, Zanos P, Georgiou P. The impact of estradiol on serotonin, glutamate, and dopamine systems. *Front. Neurosci.* 2024, 18:1348551.

[11] Mooradian AD. Antioxidant properties of steroids. *J. Steroid Biochem. Mol. Biol.* 1993, 45(6):509–511.

[12] Moosmann B, Behl C. The antioxidant neuroprotective effects of estrogens and phenolic compounds are independent from their estrogenic properties. *Proc. Natl. Acad. Sci. U.S.A.* 1999, 96(16):8867–8872.

[13] Dantas APV, Tostes RC, Fortes ZB, Costa SG, Nigro D, *et al.* In vivo evidence for antioxidant potential of estrogen in microvessels of female spontaneously hypertensive rats. *Hypertension* 2002, 39(2):405–411.

[14] Abbas AM, Elsamanoudy AZ. Effects of 17β-estradiol and antioxidant administration on oxidative stress and insulin resistance in ovariectomized rats. *Can. J. Physiol. Pharmacol.* 2011, 89(7):497–504.

[15] Prokai L, Rivera-Portalatin NM, Prokai-Tatrai K. Quantitative structure-activity relationships predicting the antioxidant potency of 17β-estradiol-related polycyclic phenols to inhibit lipid peroxidation. *Int. J. Mol. Sci.* 2013, 14(1):1443–1454.

[16] Prokai-Tatrai K, Prokai L, Simpkins JW, Jung ME. Phenolic compounds protect cultured hippocampal neurons against ethanol-withdrawal induced oxidative stress. *Int. J. Mol. Sci.* 2009, 10(4):1773–1787.

[17] Prokai L, Prokai-Tatrai K, Perjesi P, Zharikova AD, Perez EJ, *et al.* Quinol-based cyclic antioxidant mechanism in estrogen neuroprotection. *Proc. Natl. Acad. Sci. U.S.A.* 2003, 100(20):11741–11746.

[18] Römer W, Oettel M, Menzenbach B, Droescher P, Schwarz S. Novel estrogens and their radical scavenging effects, iron-chelating, and total antioxidative activities: 17α-substituted analogs of Δ9(11)-dehydro-17β-estradiol. *Steroids* 1997, 62(11):688–694.

[19] Diehl DJ, Gershon S. The role of dopamine in mood disorders. *Compr. Psychiatry* 1992, 33(2):115–120.

[20] Beninger RJ. The role of dopamine in locomotor activity and learning. *Brain Res. Rev.* 1983, 6(2):173–196.

[21] Belujon P, Grace AA. Dopamine system dysregulation in major depressive disorders. *Int. J. Neuropsychopharmacol* 2017, 20(12):1036–1046.

[22] Clos M, Bunzeck N, Sommer T. Dopamine is a double-edged sword: dopaminergic modulation enhances memory retrieval performance but impairs metacognition. *Neuropsychopharmacology* 2019, 44(3):555–563.

[23] Franco R, Reyes-Resina I, Navarro G. Dopamine in health and disease: much more than a neurotransmitter. *Biomedicines* 2021, 9(2):109.

[24] Klein MO, Battagello DS, Cardoso AR, Hauser DN, Bittencourt JC, *et al.* Dopamine: functions, signaling, and association with neurological diseases. *Cell. Mol. Neurobiol.* 2019, 39(1):31–59.

[25] Grinevich VP, Zakirov AN, Berseneva UV, Gerasimova EV, Gainetdinov RR, *et al.* Applying a fast-scan cyclic voltammetry to explore dopamine dynamics in animal models of neuropsychiatric disorders. *Cells* 2022, 11(9):1533.

[26] Shams WM, Cossette MP, Shizgal P, Brake WG. 17β-estradiol locally increases phasic dopamine release in the dorsal striatum. *Neurosci. Lett.* 2018, 665:29–32.

[27] Jacobs E, D'Esposito M. Estrogen shapes dopamine-dependent cognitive processes: implications for women's health. *J. Neurosci.* 2011, 31(14):5286–5293.

[28] Yoest KE, Cummings JA, Becker JB. Estradiol, dopamine and motivation. *Cent. Nerv. Syst. Agents*

Med. Chem. 2014, 14(2):83–89.

[29] Marinelli M, McCutcheon JE. Heterogeneity of dopamine neuron activity across traits and states. *Neuroscience* 2014, 282:176–197.

[30] Rafi H, Zestos AG. Review—recent advances in FSCV detection of neurochemicals via waveform and carbon microelectrode modification. *J. Electrochem. Soc.* 2021, 168(5):057520.

[31] Bard AJ, Faulkner LR, White HS. *Electrochemical Methods: Fundamentals and Applications*, 3rd ed. Hoboken: John Wiley & Sons,2022.

[32] Musa AM, Kiely J, Luxton R, Honeychurch KC. Recent progress in screen-printed electrochemical sensors and biosensors for the detection of estrogens. *TrAC Trends Anal. Chem.* 2021, 139:116254.

[33] Musa AM, Kiely J, Luxton R, Honeychurch KC. Graphene-based electrodes for monitoring of estradiol. *Chemosensors* 2023, 11(6):337.

[34] Lu X, Sun J, Sun X. Recent advances in biosensors for the detection of estrogens in the environment and food. *TrAC Trends Anal. Chem.* 2020, 127:115882.

[35] Robinson DL, Hermans A, Seipel AT, Wightman RM. Monitoring rapid chemical communication in the brain. *Chem. Rev.* 2008, 108(7):2554–2584.

[36] Simonsson L, Kurczy ME, Trouillon R, Hook F, Cans AS. A functioning artificial secretory cell. *Sci. Rep.* 2012, 2(1):824.

[37] Puthongkham P, Venton BJ. Recent advances in fast-scan cyclic voltammetry. *Analyst* 2020, 145(4):1087–1102.

[38] Venton BJ, Cao Q. Fundamentals of fast-scan cyclic voltammetry for dopamine detection. *Analyst* 2020, 145(4):1158–1168.

[39] Wightman RM, May LJ, Michael AC. Detection of dopamine dynamics in the brain. *Anal. Chem.* 1988, 60(13):769A–779A.

[40] Bath BD, Michael DJ, Trafton BJ, Joseph JD, Runnels PL, *et al.* Subsecond adsorption and desorption of dopamine at carbon-fiber microelectrodes. *Anal. Chem.* 2000, 72(24):5994–6002.

[41] Heien MLAV, Phillips PEM, Stuber GD, Seipel AT, Wightman RM. Overoxidation of carbon-fiber microelectrodes enhances dopamine adsorption and increases sensitivity. *Analyst* 2003, 128(12):1413–1419.

[42] Venton BJ, Michael DJ, Wightman RM. Correlation of local changes in extracellular oxygen and pH that accompany dopaminergic terminal activity in the rat caudate–putamen. *J. Neurochem.* 84(2):373–381.

[43] Keithley RB, Takmakov P, Bucher ES, Belle AM, Owesson-White CA, *et al.* Higher sensitivity dopamine measurements with faster-scan cyclic voltammetry. *Anal. Chem.* 2011, 83(9):3563–3571.

[44] Heien MLAV, Johnson MA, Wightman RM. Resolving neurotransmitters detected by fast-scan cyclic voltammetry. *Anal. Chem.* 2004, 76(19):5697–5704.

[45] Shon YM, Chang SY, Tye SJ, Kimble CJ, Bennet KE, *et al.* Comonitoring of adenosine and dopamine using the wireless instantaneous neurotransmitter concentration system: proof of principle. *J. Neurosurg.* 2010, 112(3):539–548.

[46] Paek SB, Knight EJ, Chang SY, Lujan JL, Jang DP, *et al.* Dopamine measurement during prolonged deep brain stimulation: a proof-of-principle study of paired pulse voltammetry. *Biomed. Eng. Lett.* 2013, 3(1):22–31.

[47] Grahn PJ, Mallory GW, Khurram OU, Berry BM, Hachmann JT, *et al.* A neurochemical closed-loop controller for deep brain stimulation: toward individualized smart neuromodulation therapies. *Front. Neurosci.* 2014, 8:169.

[48] Chang SY, Shon YM, Agnesi F, Lee KH. Microthalamotomy effect during deep brain stimulation: potential involvement of adenosine and glutamate efflux. In *2009 Annual International Conference of the IEEE Engineering in Medicine and Biology Society*, Minneapolis, USA, September 03–06, 2009, pp. 3294–3297.

[49] Chang SY, Kim I, Marsh MP, Jang DP, Hwang SC, *et al.* Wireless fast-scan cyclic voltammetry to monitor adenosine in patients with essential tremor during deep brain stimulation. *Mayo Clin. Proc.* 2012, 87(8):760–765.

[50] Corva DM, Parke B, West A, Doeven EH, Adams SD, *et al.* SmartStim: an artificial intelligence enabled deep brain stimulation device. *IEEE Trans. Med. Robot. Bion.* 2024, 6(2):674–684.

[51] Weese-Myers ME, Ross AE. Electrochemical characterization of 17β-estradiol with fast-scan cyclic voltammetry. *Electroanalysis* 2023, 35(9):e202200560.

[52] Weese-Myers ME, Ross AE. Subsecond codetection of dopamine and estradiol at a modified sharkfin waveform. *Anal. Chem.* 2024, 96(1):76–84.

[53] Römer W, Oettel M, Menzenbach B, Droescher P, Schwarz S. Novel estrogens and their radical scavenging effects, iron-chelating, and total antioxidative activities: 17-substituted analogs of 9(11)-dehydro-17-estradiol. *Steroids* 1997, 62(11):688–694.

[54] Harreither W, Trouillon R, Poulin P, Neri W, Ewing AG, *et al.* Cysteine residues reduce the severity of dopamine electrochemical fouling. *Electrochim. Acta.* 2016, 210:622–629.

[55] Monzani E, Nicolis S, Dell'Acqua S, Capucciati A, Bacchella C, *et al.* Dopamine, oxidative stress and protein–quinone modifications in Parkinson's and other neurodegenerative diseases. *Angew. Chem. Int. Ed.* 2019, 58(20):6512–6527.

[56] Cahill PS, Walker QD, Finnegan JM, Mickelson GE, Travis ER, *et al.* Microelectrodes for the measurement of catecholamines in biological systems. *Anal. Chem.* 68(18):3180–3186.

[57] Zachek MK, Hermans A, Wightman RM, McCarty GS. Electrochemical dopamine detection: comparing gold and carbon fiber microelectrodes using background subtracted fast scan cyclic voltammetry. *J. Electroanal. Chem.* 2008, 614(1-2):113–120.

[58] Trouillon R, Gijs MAM. Dynamic electrochemical quantitation of dopamine release from a cells-on-paper system. *RSC Adv.* 2016, 6(37):31069–31073.

[59] Trouillon R, Gijs MAM. Delayed voltammetric with respect to amperometric electrochemical detection of concentration changes in microchannels. *Lab Chip.* 2014, 14:2929–2940.

[60] Caux M, Achit A, Var K, Boitel-Aullen G, Rose D, *et al.* PassStat, a simple but fast, precise and versatile open source potentiostat. *HardwareX* 2022, 11:e00290.

[61] Pelletier J, Trouillon R. Tuning the properties of paper-based electrodes for neurochemical analysis. *Electrochim. Acta.* 2024, 475:143528.

[62] Trouillon R, Gijs MAM. Cells-on-electrode-on-paper: analytical platforms for the chemical study of cellular secretion. *Biosens. Bioelectron.* 2023, 14:100327.

[63] Ezzati R. Derivation of pseudo-first-order, pseudo-second-order and modified pseudo-first-order rate equations from Langmuir and Freundlich isotherms for adsorption. *Chem. Eng. J.* 2020, 392:123705.

[64] Long GL, Winefordner JD. Limit of detection a closer look at the IUPAC definition. *Anal. Chem.* 1983, 55(07):712A–724A.

[65] Ngundi MM, Sadik OA, Yamaguchi T, Suye SI. First comparative reaction mechanisms of β-estradiol and selected environmental hormones in a redox environment. *Electrochem. Commun.* 2003, 5(1):61–67.

[66] Wong A, Santos AM, Fava EL, Fatibello-Filho O, Sotomayor MDPT. Voltammetric determination of 17β-estradiol in different matrices using a screen-printed sensor modified with CuPc, Printex 6L carbon and Nafion film. *Microchem. J.* 2019, 147:365–373.

[67] Supchocksoonthorn P, Alvior Sinoy MC, de Luna MDG, Paoprasert P. Facile fabrication of 17β-estradiol electrochemical sensor using polyaniline/carbon dot-coated glassy carbon electrode with synergistically enhanced electrochemical stability. *Talanta* 2021, 235:122782.

[68] Yılmaz B, Kadıoğlu Y. Electrochemical study of 17β-estradiol and its determination in pharmaceutical preparations using square wave voltammetry. *J. Turk. Chem. Soc. Ser. A.* 2023, 10(3):589–598.

[69] Galvão JCR, Araujo MdS, Prete MC, Neto VL, Dall'Antonia LH, *et al.* Electrochemical determination of 17-β-estradiol using a glassy carbon electrode modified with α-Fe2O3 nanoparticles supported on carbon nanotubes. *Molecules* 2023, 28(17):6372.

[70] McCreery RL. Advanced carbon electrode materials for molecular electrochemistry. *Chem. Rev.* 2008, 108(7):2646–2687.

[71] Trouillon R, O'Hare D, Einaga Y. Effect of the doping level on the biological stability of hydrogenated boron doped diamond electrodes. *Phys. Chem. Chem. Phys.* 2011, 13:5422–5429.

[72] Trouillon R, Einaga Y, Gijs MA. Cathodic pretreatment improves the resistance of boron-doped diamond electrodes to dopamine fouling. *Electrochem. Commun.* 2014, 47:92–95.

[73] B AK, Bhat VS, Varghese A, George L, Hegde G. Non-enzymatic electrochemical determination of progesterone using carbon nanospheres from onion peels coated on carbon fiber paper. *J. Electrochem. Soc.* 2019, 166(13):B1097.

[74] Takmakov P, Zachek MK, Keithley RB, Walsh PL, Donley C, *et al.* Carbon microelectrodes with a renewable surface. *Anal. Chem.* 2010, 82(5):2020–2028.

[75] Roberts JG, Moody BP, McCarty GS, Sombers LA. Specific oxygen-containing functional groups on the carbon surface underlie an enhanced sensitivity to dopamine at electrochemically pretreated carbon fiber microelectrodes. *Langmuir* 2010, 26(11):9116–9122.

[76] Häring AP, Pollok D, Strücker BR, Kilian V, Schneider J, *et al.* Beyond Kolbe and Hofer–Moest: electrochemical synthesis of carboxylic anhydrides from carboxylic acids. *ChemistryOpen* 2022, 11(5):e202200059.

[77] Rodeberg NT, Sandberg SG, Johnson JA, Phillips PEM, Wightman RM. Hitchhiker's guide to voltammetry: acute and chronic electrodes for in vivo fast-scan cyclic voltammetry. *ACS Chem. Neurosci.* 2017, 8(2):221–234.

[78] Olufunmilayo EO, Gerke-Duncan MB, Holsinger RMD. Oxidative stress and antioxidants in neurodegenerative disorders. *Antioxidants* 2023, 12(2):517.

[79] Saunders-Pullman R, Gordon-Elliott J, Parides M, Fahn S, Saunders H, *et al.* The effect of estrogen replacement on early Parkinson's disease. *Neurology* 1999, 52(7):1417–1417.